
Temporally-Reweighted Chinese Restaurant Process Mixtures for Clustering, Imputing, and Forecasting Multivariate Time Series

Feras A. Saad

Probabilistic Computing Project
Massachusetts Institute of Technology

Vikash K. Mansinghka

Probabilistic Computing Project
Massachusetts Institute of Technology

Abstract

This article proposes a Bayesian nonparametric method for forecasting, imputation, and clustering in sparsely observed, multivariate time series data. The method is appropriate for jointly modeling hundreds of time series with widely varying, non-stationary dynamics. Given a collection of N time series, the Bayesian model first partitions them into independent clusters using a Chinese restaurant process prior. Within a cluster, all time series are modeled jointly using a novel “temporally-reweighted” extension of the Chinese restaurant process mixture. Markov chain Monte Carlo techniques are used to obtain samples from the posterior distribution, which are then used to form predictive inferences. We apply the technique to challenging forecasting and imputation tasks using seasonal flu data from the US Center for Disease Control and Prevention, demonstrating superior forecasting accuracy and competitive imputation accuracy as compared to multiple widely used baselines. We further show that the model discovers interpretable clusters in datasets with hundreds of time series, using macroeconomic data from the Gapminder Foundation.

there are tens or hundreds of time series. One challenge in these settings is that the data may reflect underlying processes with widely varying, non-stationary dynamics [13]. Another challenge is that standard parametric approaches such as state-space models and vector autoregression often become statistically and numerically unstable in high dimensions [20]. Models from these families further require users to perform significant custom modeling on a per-dataset basis, or to search over a large set of possible parameter settings and model configurations. In econometrics and finance, there is an increasing need for multivariate methods that exploit sparsity, are computationally efficient, and can accurately model hundreds of time series (see introduction of [15], and references therein).

This paper presents a nonparametric Bayesian method for multivariate time series that aims to address some of the above challenges. The model is based on two extensions to Dirichlet process mixtures. First, we introduce a recurrent version of the Chinese restaurant process mixture to capture temporal dependences. Second, we add a hierarchical prior to discover groups of time series whose underlying dynamics are modeled jointly. Unlike autoregressive models, our approach is designed to interpolate in regimes where it has seen similar history before, and reverts to a broad prior in previously unseen regimes. This approach does not sacrifice predictive accuracy, when there is sufficient signal to make a forecast or impute missing data.

We apply the method to forecasting flu rates in 10 US regions using flu, weather, and Twitter data from the US Center for Disease Control and Prevention. Quantitative results show that the method outperforms several Bayesian and non-Bayesian baselines, including Facebook Prophet, multi-output Gaussian processes, seasonal ARIMA, and the HDP-HMM. We also show competitive imputation accuracy with widely used statistical techniques. Finally, we apply the method to clustering hundreds of macroeconomic time series from Gapminder, detecting meaningful clusters of countries whose data exhibit coherent temporal patterns.

1 Introduction

Multivariate time series data is ubiquitous, arising in domains such as macroeconomics, neuroscience, and public health. Unfortunately, forecasting, imputation, and clustering problems can be difficult to solve when

Proceedings of the 21st International Conference on Artificial Intelligence and Statistics (AISTATS) 2018, Lanzarote, Spain. PMLR: Volume 84. Copyright 2018 by the author(s).

2 Related Work

The temporally-reweighted Chinese restaurant process (TRCRP) mixture we introduce in Section 3 can be directly seen as a time series extension to a family of nonparametric Bayesian regression models for cross-sectional data [18, 35, 28, 22, 23]. These methods operate on an exchangeable data sequence $\{x_i\}$ with exogenous covariates $\{\mathbf{y}_i\}$; the prior CRP cluster probability $p(z_i = k)$ for each observation x_i is reweighted based on \mathbf{y}_i . Our method extends this idea to a time series $\{x_t\}$; the prior CRP cluster probability $p(z_t = k)$ for x_t is now reweighted based on the p previous values $\mathbf{x}_{t-1:t-p}$. Moreover, the hierarchical extension in Section 3.4 coincides with CrossCat [21], when all temporal dependencies are removed (by setting $p = 0$).

Temporal extensions to the Dirichlet process have been previously used in the context of dynamic clustering [38, 1]. The latter work derives a recurrent CRP as the limit of a finite dynamic mixture model. Unlike the method in this paper, those models are used for clustering batched data and dynamic topic modeling [7], rather than data analysis tasks such as forecasting or imputation in real-valued, multivariate time series.

For multivariate time series, recent nonparametric Bayesian methods include using the dependent Dirichlet process for dynamic density estimation [31]; hierarchical DP priors over the state in hidden Markov models [HDP-HMM; 12, 19]; Pitman-Yor mixtures of non-linear state-space models for clustering [26]; and DP mixtures [8] and Polya trees [27] for modeling noise distributions. As nonparametric Bayesian extensions of state-space models, all of these approaches specify priors that fall under distinct model classes to the one developed in this paper. They typically encode parametric assumptions (such as linear autoregression and hidden-state transition matrices), or integrate explicit specifications of underlying temporal dynamics such as seasonality, trends, and time-varying functionals. Our method instead builds purely empirical models and uses simple infinite mixtures to detect patterns in the data, without relying on dataset-specific customizations. As a multivariate interpolator, the TRCRP mixture is best applied to time series where there is no structural theory of the temporal dynamics, and where there is sufficient statistical signal in the history of the time series to inform probable future values.

To the best of our knowledge, this paper presents the first multivariate, nonparametric Bayesian model that provides strong baseline results without specifying custom dynamics on a problem-specific basis; and that has been benchmarked against multiple Bayesian and non-Bayesian techniques to cluster, impute, and forecast sparsely observed real-world time series data.

3 Temporally-Reweighted Chinese Restaurant Process Mixture Model

We first outline the notations and basic setup assumed throughout this paper. Let $\{\mathbf{x}^n : n = 1, \dots, N\}$ denote a collection of N discrete-time series, where the first T variables of the n^{th} time series is $\mathbf{x}_{1:T}^n = (x_1^n, x_2^n, \dots, x_T^n)$. Slice notation is used to index subsequences of variables, so that $\mathbf{x}_{t_1:t_2}^n = (x_{t_1}^n, \dots, x_{t_2}^n)$ for $t_1 < t_2$. Superscript n will be often be omitted when discussing a single time series. The remainder of this section develops a generative process for the joint distribution of all random variables $\{x_t^n : t = 1, \dots, N, n = 1, \dots, N\}$ in the N time series, which we proceed to describe in stages.

3.1 Background: CRP representation of Dirichlet process mixture models

Our approach is based on a temporal extension of the standard Dirichlet process mixture (DPM), which we review briefly. First consider the standard DPM in the non-temporal setting [11], with concentration α and base measure π_Θ . The joint distribution of a sequence of m exchangeable random variables (x_1, \dots, x_m) is:

$$P \sim DP(\alpha, \pi_\Theta), \quad \theta_j^* | P \sim P, \quad x_j | \theta_j^* \sim F(\cdot | \theta_j^*).$$

The DPM can be represented in terms of the Chinese restaurant process [2]. As P is almost-surely discrete, the m draws $\{\theta_j^*\} \sim P$ contain repeated values, thereby inducing a clustering among data x_j . Let λ_F be the hyperparameters of π_Θ , $\{\theta_k\}$ be the unique values among the $\{\theta_j^*\}$, and z_j denote the cluster assignment of x_j which satisfies $\theta_j^* = \theta_{z_j}$. Define n_{jk} to be the number of observations x_i with $z_i = k$ for $i < j$. Using the conditional distribution of z_j given previous cluster assignments $\mathbf{z}_{1:j-1}$, the joint distribution of exchangeable data sequence (x_1, x_2, \dots) in the CRP mixture model can be described sequentially:

$$\begin{aligned} \{\theta_k\} &\stackrel{\text{iid}}{\sim} \pi_\Theta(\cdot | \lambda_F) \\ \Pr[z_j = k | \mathbf{z}_{1:j-1}; \alpha] & \quad (j = 1, 2, \dots) \\ &\propto \begin{cases} n_{jk} & \text{if } 1 \leq k \leq \max(\mathbf{z}_{1:j-1}) \\ \alpha & \text{if } k = \max(\mathbf{z}_{1:j-1}) + 1 \end{cases} \end{aligned} \tag{1}$$

$$x_j | z_j, \{\theta_k\} \sim F(\cdot | \theta_{z_j})$$

The CRP mixture model (1), and algorithms for posterior inference, have been studied extensively for nonparametric modeling in a variety of statistical applications (for a survey see [37], and references therein).

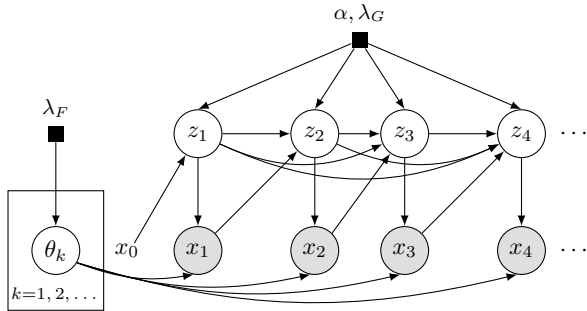


Figure 1: Graphical model for the TRCRP mixture in a single time series $\mathbf{x} = (x_1, x_2, \dots)$ with lagged window size $p = 1$.

3.2 The temporally-reweighted CRP mixture for modeling a single time series

Our objective is to define a CRP-like process for a non-exchangeable discrete-time series (x_1, x_2, \dots) , where there is now a temporal ordering and a temporal dependence among the variables. Instead of having (x_t, z_t) be conditionally independent of all other data given $\mathbf{z}_{1:t-1}$ as in the CRP mixture (1), we instead consider using previous observations $\mathbf{x}_{1:t-1}$ when simulating z_t . The main idea in our approach is to modify the CRP prior by having the cluster probability $\Pr[z_t = k \mid \mathbf{z}_{1:t-1}]$ at step t additionally account for (i) the p most recent observations $\mathbf{x}_{t-p:t-1}$, and (ii) collection of lagged values $D_{tk} := \{\mathbf{x}_{t'-p:t'-1} \mid z_{t'} = k, 1 \leq t' < t\}$ of earlier data points $x_{t'}$ assigned to cluster k . The distribution of time series (x_1, x_2, \dots) in the temporally-reweighted CRP (TRCRP) mixture is therefore:

$$\begin{aligned} \{\theta_k\} &\stackrel{\text{iid}}{\sim} \pi_{\Theta}(\cdot \mid \lambda_F) \\ \Pr[z_t = k \mid \mathbf{z}_{1:t-1}, \mathbf{x}_{t-p:t-1}; \alpha, \lambda_G] &\quad (t = 1, 2, \dots) \\ &\propto \begin{cases} n_{tk} G(\mathbf{x}_{t-p:t-1}; D_{tk}, \lambda_G) & \text{if } 1 \leq k \leq \max(\mathbf{z}_{1:t-1}) \\ \alpha G(\mathbf{x}_{t-p:t-1}; \lambda_G) & \text{if } k = \max(\mathbf{z}_{1:t-1}) + 1 \end{cases} \\ x_t \mid z_t, \{\theta_k\} &\sim F(\cdot \mid \theta_{z_t}) \end{aligned} \quad (2)$$

The main difference between the TRCRP mixture (2) and the standard CRP mixture (1) is the term $G(\mathbf{x}_{t-p:t-1}; \lambda_G, D_{tk})$ which acts as a non-negative “cohesion” function $\mathbb{R}^p \rightarrow \mathbb{R}^+$, parametrized by D_{tk} and a bundle of real values λ_G . This term measures how well the current lagged values $\mathbf{x}_{t-p:t-1}$ match the collection of lagged values of earlier data D_{tk} in each cluster k , thereby introducing temporal dependence to the model. The smoothness of the process depends on the choice of the window size p : if t_1 and t_2 are close in time (relative to p) then they have overlapping lagged values $\mathbf{x}_{t_1-p:t_1-1}$ and $\mathbf{x}_{t_2-p:t_2-1}$, so G increases the prior probability that $\{z_{t_1} = z_{t_2}\}$. More generally, any pair of time points t_1 and t_2 that share similar lagged

values are a-priori more likely to have similar distributions for generating x_{t_1} and x_{t_2} , because G increases the probability that $\{z_{t_1} = z_{t_2} = k\}$, so that x_{t_1} and x_{t_2} are both drawn from $F(\cdot \mid \theta_k)$.

Figure 1 shows a graphical model for the TRCRP mixture (2) with window size $p = 1$. The model proceeds as follows: first assume the initial p observations (x_{-p+1}, \dots, x_0) are fixed or have a known joint distribution. At step t , the generative process samples a cluster assignment z_t , whose probability of joining cluster k is a product of (i) the CRP probability for $\{z_t = k\}$ given all previous cluster assignments $\mathbf{z}_{1:t-1}$, and (ii) the “cohesion” term $G(\mathbf{x}_{t-p:t-1}; \lambda_G, D_{tk})$. In Figure 1, edges between the z_t ’s denote the CRP probabilities, while edges from x_{t-1} up to z_t represent reweighting the CRP by G . Cluster assignment z_t identifies the temporal regime that dictates the distribution of $x_t \sim F(\cdot \mid \theta_{z_t})$. Observe that if $p = 0$ or $G \propto 1$, then the model reduces to a standard CRP mixture (1) with no temporal dependence, since (z_t, x_t) are conditionally independent of the entire time series history $\mathbf{x}_{1:t-1}$ given $\mathbf{z}_{1:t-1}$. Also note that the model is not Markovian, due to the infinite coupling among the latent z_t (compare to the recurrent switching linear dynamical system of [4]).

The data distribution F in (2) is a Normal distribution with Normal-InverseGamma prior π_{Θ} :

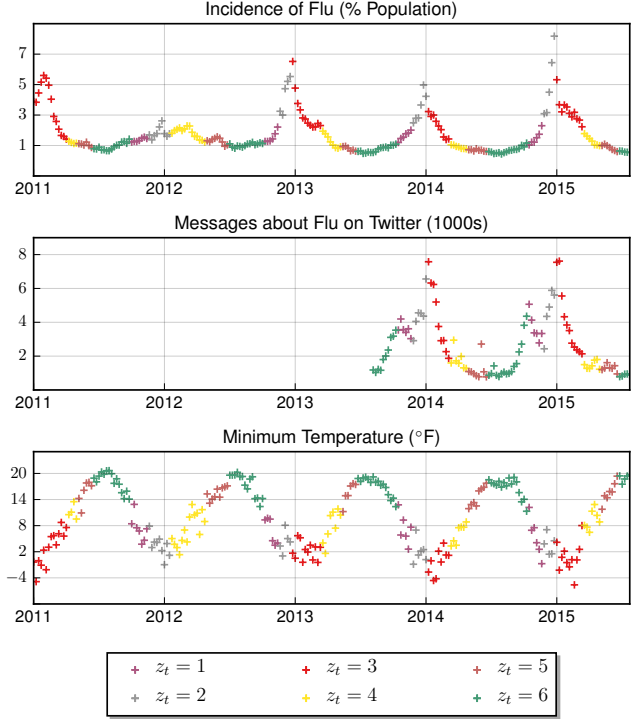
$$\begin{aligned} \pi_{\Theta}(\mu_k, \sigma_k^2 \mid m, V, a, b) &= \text{N}(\mu_k \mid m, \sigma_k^2 V) \text{IG}(\sigma_k^2 \mid a, b) \\ F(x_t \mid \mu_k, \sigma_k^2) &= \text{N}(x_t \mid \mu_k, \sigma_k^2), \end{aligned} \quad (3)$$

where $\theta_k = (\mu_k, \sigma_k^2)$ are the per-cluster parameters of F , and $\lambda_F = (m, V, a, b)$ the hyperparameters of π_{Θ} . Conjugacy of F and π_{Θ} [5] implies that θ_k can be marginalized out of the generative model (2) (see Appendix B). As for G , it may in general be any non-negative weighting function which assigns a high value to lagged data vectors that are “similar” to one another. Previous approaches Bayesian nonparametric regression constructed covariate-dependent probability measures using kernel-based reweighting [10]. Our method defines G as a product of p Student-T distributions whose location, scale, and degrees of freedom depend on lagged data D_{tk} in cluster k :

$$\begin{aligned} G(\mathbf{x}_{t-p:t-1}; D_{tk}, \lambda_G) &= \prod_{i=1}^p G_i(x_{t-i}; D_{tki}, \lambda_{Gi}) \\ &= \prod_{i=1}^p \text{T}_{2a_{tki}} \left(x_{t-i}; m_{tki}, b_{tki} \frac{1 + V_{tki}}{a_{tki}} \right) \end{aligned} \quad (4)$$

where hyperparameter $\lambda_{Gi} = (m_{i0}, V_{i0}, a_{i0}, V_{i0})$ and data $D_{tki} = \{x_{t'-i} : z_{t'} = k, 1 \leq t' < t\}$. Equations for the data-dependent terms $(m_{tki}, V_{tki}, a_{tki}, b_{tki})$ are given in Appendix A. We emphasize that G itself is

1. Sample concentration parameter of CRP
 $\alpha \sim \text{Gamma}(1,1)$
2. Sample model hyperparameters $(n = 1, 2, \dots, N)$
 $\lambda_G^n \sim H_G^n$
 $\lambda_F^n \sim H_F^n$
3. Sample distribution parameters of F $(n = 1, 2, \dots, N)$
 $\theta_1^n, \theta_2^n, \dots \stackrel{\text{iid}}{\sim} \pi_\Theta(\cdot | \lambda_F^n)$
4. Assume first p values are known $(n = 1, 2, \dots, N)$
 $\mathbf{x}_{-p+1:0}^n := (x_{-p+1}^n, \dots, x_0^n)$
5. Sample time series observations $(t = 1, 2, \dots)$
 - 5.1 Sample temporal cluster assignment z_t
 $\Pr [z_t = k | \mathbf{z}_{1:t-1}, \mathbf{x}_{t-p:t-1}^{1:N}, \alpha, \lambda_G^{1:N}]$
 $\propto \text{CRP}(k | \alpha, \mathbf{z}_{1:t-1}) \prod_{n=1}^N G(\mathbf{x}_{t-p:t-1}^n; D_{tk}^n, \lambda_G^n)$
 where $D_{tk}^n := \{\mathbf{x}_{t'-p:t'-1}^n | z_{t'} = k, 1 \leq t' < t\}$
 and $k = 1, \dots, \max(\mathbf{z}_{1:t-1}) + 1$
 - 5.2 Sample data x_t^n $(n = 1, 2, \dots, N)$
 $x_t^n | z_t, \{\theta_k^n\} \sim F(\cdot | \theta_{z_t}^n)$



(a) Generative process for the multivariate TRCRP mixture (b) Discovering flu season dynamics with the method

Figure 2: (a) Generative model describing the joint distribution of N dependent time series $\{\mathbf{x}^n\}$ in the multivariate temporally-reweighted CRP mixture. Lagged values for all time series are used for reweighting the CRP by G in step 5.1. Dependencies between time series are mediated by the shared temporal regime assignment z_t , which ensures that all the time series have the same segmentation of the time course into the different temporal regimes. (b) Applying the TRCRP mixture with $p = 10$ weeks to model \mathbf{x}^{flu} , $\mathbf{x}^{\text{tweet}}$, and \mathbf{x}^{temp} in US Region 4. Six regimes describing the seasonal behavior shared among the three time series are detected in this posterior sample. Purple, gray, and red are the pre-peak rise, peak, and post-peak decline during the flu season; and yellow, brown, and green represent the rebound in between successive seasons. In 2012, the model reports no red post-peak regime, reflecting the season’s mild flu peak. See Section 5 for quantitative experiments.

used for reweighting only; it does not define a probability distribution over lagged data. Mathematically, G attracts x_t towards a cluster k that assigns $\mathbf{x}_{t-p:t-1}$ a high density, under the posterior predictive of an axis-aligned Gaussian having observed D_{tk} [24].

3.3 Extending the TRCRP mixture to multiple dependent time series

This section generalizes the univariate TRCRP mixture (2) to handle a collection of N time series $\{\mathbf{x}^n : n = 1, \dots, N\}$, assumed for now to all be dependent. At time t , we let the temporal regime assignment z_t be shared among all the time series, and use lagged values of all N time series when reweighting the CRP probabilities by the cohesion term G . Figure 2a contains a step-by-step description of the multivariate TRCRP mixture, with an illustrative application in Figure 2b. It is informative to consider how z_t mediates dependences between $\mathbf{x}^{1:N}$. First, the model

requires all time series to be in the same regime z_t at time t . However, each time series has its own set of per-cluster parameters $\{\theta_k^n\}$. Therefore, all the time series share the same segmentation $\mathbf{z}_{1:T}$ of the time course into various temporal regimes, even though the parametric distributions $F(\cdot | \theta_k^n), n = 1, \dots, N$ within each temporal regime $k \in \mathbf{z}_{1:T}$ differ. Second, the model makes the “naive Bayes” assumption that data $\{x_t^n\}_{n=1}^N$ at time t are independent given z_t , and that the reweighting term G in step 5.1 factors as a product. This characteristic is essential for numerical stability of the method in high dimensional and sparse regimes, while still maintaining the ability to recover complex distributions due to the infinite CRP mixture.

3.4 Learning the dependence structure between multiple time series

The TRCRP mixture in Figure 2a makes the restrictive assumption that all time series $\mathbf{x}^{1:N}$ are dependent

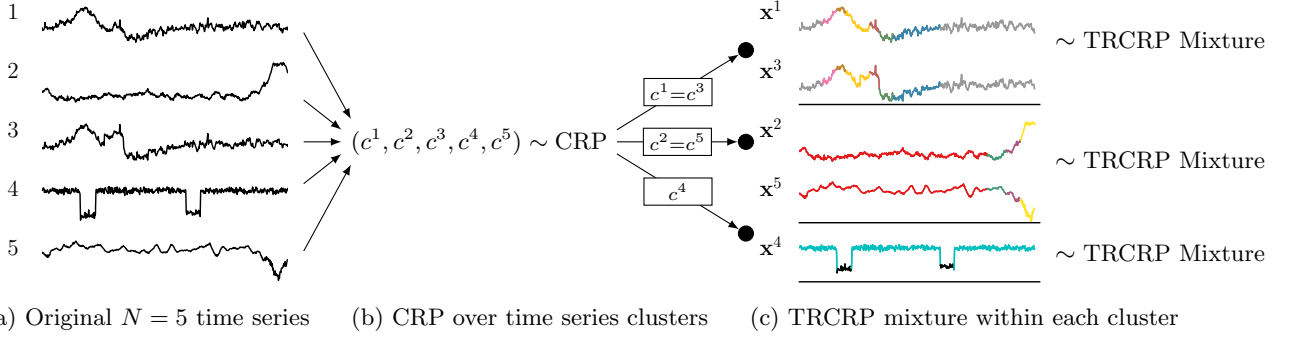


Figure 3: Hierarchical prior for learning the dependence structure between multiple time series. Given N EEG time series, we first nonparametrically partition them by sampling an assignment vector $\mathbf{c}^{1:N}$ from an “outer” CRP. Time series assigned to the same cluster are jointly generated using the TRCRP mixture. Colored segments of each curve indicate the hidden states at each time step (the shared latent variables within the cluster).

with one another. However, with dozens or hundreds of time series whose temporal regimes are not well-aligned, forcing a single segmentation sequence $\mathbf{z}_{1:T}$ to apply to all N time series will result in a poor fit to the data. We relax this assumption by introducing a hierarchical prior that allows the model to determine which subsets of the N time series are probably well-described by a joint TRCRP model. The prior induces sparsity in the dependencies between the N time series by first nonparametrically partitioning them using an “outer” CRP. Within a cluster, all time series are modeled jointly using the multivariate TRCRP mixture described in Figure 2a:

$$\begin{aligned} (c^1, c^2, \dots, c^N) &\sim \text{CRP}(\cdot | \alpha_0) \\ \{\mathbf{x}^n : c^n = k\} &\sim \text{TRCRP Mixture} \\ &(k = 1, \dots, \max \mathbf{c}^{1:N}), \end{aligned} \quad (5)$$

where c^n is the cluster assignment of \mathbf{x}^n . Figure 3 shows an example of this structure learning prior applied to five EEG time series. In the second cluster of panel (c), the final yellow segment illustrates two time series sharing the latent regime at each time step, but having different distributions within each regime.

4 Posterior Inferences via Markov Chain Monte Carlo

In this section, we give the full model likelihood and briefly describe MCMC algorithms for inference in the hierarchical TRCRP mixture (5). Since the model learns $M = \max(\mathbf{c}^{1:N})$ separate TRCRP mixtures (one for each time series cluster) we superscript latent variables of Figure 2a by $m = 1, \dots, M$. Namely, α^m is the CRP concentration, and $\mathbf{z}_{1:T}^m$ the latent regime vector, shared by all time series in cluster m . Further, let $K_m = \max(\mathbf{z}_{1:T}^m)$ denote the number of unique regimes in $\mathbf{z}_{1:T}^m$. Given window size p and initial observations

$\{\mathbf{x}_{-p+1:0}^n : n = 1, \dots, N\}$, we have:

$$\begin{aligned} &P\left(\alpha_0, \mathbf{c}^{1:N}, \alpha^{1:M}, \lambda_G^{1:N}, \lambda_F^{1:N}, \{\theta_j^n : 1 \leq j \leq K_{c^n}\}_{n=1}^N, \right. \\ &\quad \left. \mathbf{z}_{1:T}^{1:M}, \mathbf{x}_{1:T}^{1:N}; \mathbf{x}_{-p+1:0}^{1:N}\right) \\ &= \Gamma(\alpha_0; 1, 1) \text{CRP}(\mathbf{c}^{1:N} | \alpha_0) \\ &\quad \left(\prod_{n=1}^N H_G^n(\lambda_G^n) \right) \left(\prod_{n=1}^N H_F^n(\lambda_F^n) \right) \left(\prod_{n=1}^N \prod_{j=1}^{K_{c^n}} \pi_{\Theta}^n(\theta_j^n) \right) \\ &\quad \prod_{m=1}^M \left(\Gamma(\alpha^m; 1, 1) \prod_{t=1}^T \left[b_t^m \text{CRP}(z_t^m | \mathbf{z}_{1:t-1}^m, \alpha^m) \right. \right. \\ &\quad \left. \left. \prod_{n|c_n=m} G(\mathbf{x}_{t-p:t-1}^n; D_{tz_t^m}^n, \lambda_G^n) F(x_t^n | \theta_{z_t^m}^n) \right] \right), \quad (6) \end{aligned}$$

where b_t^m normalizes the term between the square brackets, summed over $z_t^m = 1, \dots, \max(\mathbf{z}_{1:t-1}^m) + 1$. Eq (6) defines the unnormalized posterior distribution of all latent variables given the data. Appendix B contains detailed algorithms for posterior inference. Briefly, temporal regime assignments ($z_t^m | \mathbf{z}_{1:T}^m, \dots$) are sampled using a variant of Algorithm 3 from [25], taking care to handle the temporal-coupling term b_t^m which is not found in traditional DPM samplers. We also outline an alternative particle-learning scheme [9] to sample $(\mathbf{z}_{1:T}^m | \dots)$ jointly as a block. Time series cluster assignments $(c^n | \mathbf{c}^{1:N \setminus n}, \dots)$ are transitioned by proposing to move \mathbf{x}^n to either an existing or a new cluster, and computing the appropriate MH acceptance ratio for each case. Model hyperparameters are sampled using an empirical Bayes approach [30] and the “griddy Gibbs” [29] sampler.

4.1 Making predictive inferences

Given a collection of approximate posterior samples $\{\hat{\xi}^1, \dots, \hat{\xi}^S\}$ of all latent variables produced by S in-

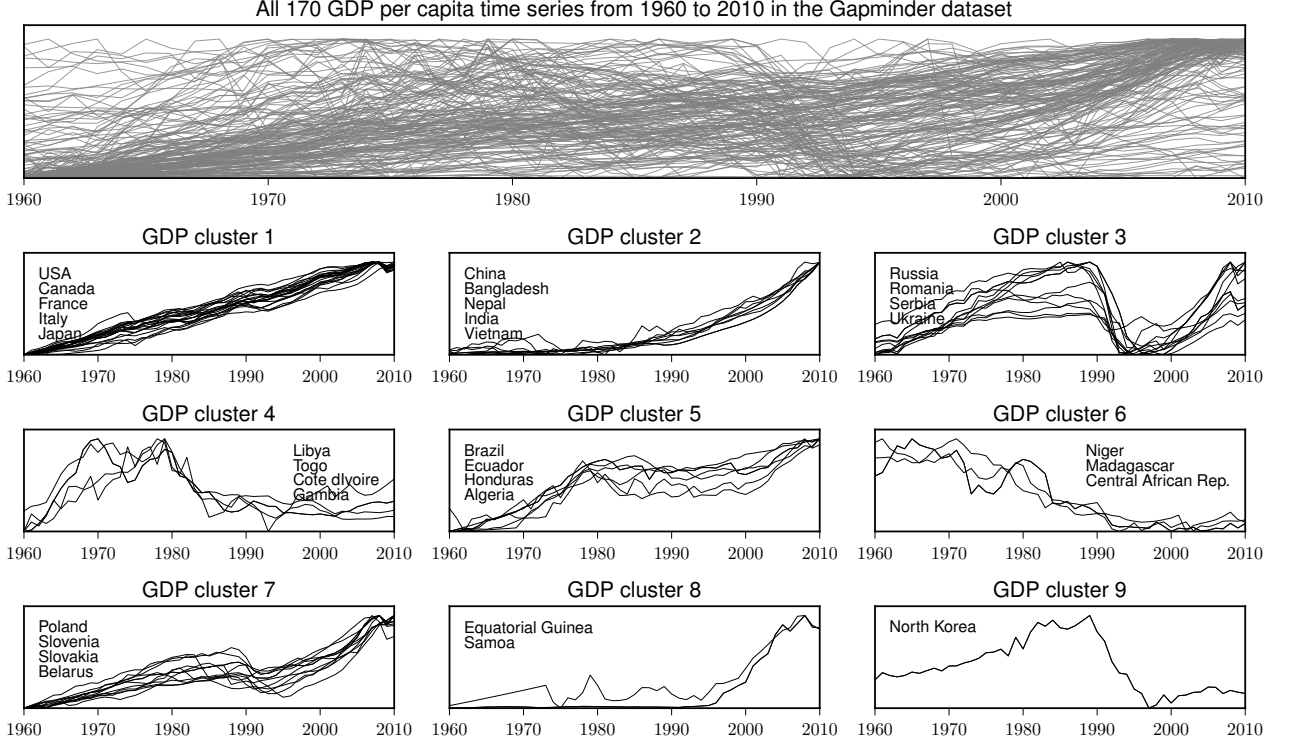


Figure 4: Given GDP per capita data for 170 countries from 1960-2010, the hierarchical TRCRP mixture (5) detects qualitatively distinct temporal patterns. The top panel shows an overlay of all the time series; nine representative clusters averaged over 60 posterior samples are shown below. Countries within each cluster, of which a subset are labeled, share similar political, economic, and/or geographic characteristics. For instance, cluster 1 contains Western democracies with stable economic growth over 50 years (slight dip in 2008 is the financial crash). Cluster 2 includes China and India, whose GDP growth rates have outpaced those of industrialized nations since the 1990s. Cluster 3 contains former communist nations, whose economies tanked after fall of the Soviet Union. Outliers such as Samoa, Equatorial Guinea, and North Korea can be seen in clusters 8 and 9.

dependent runs of MCMC, we can draw a variety of predictive inferences about the time series $\mathbf{x}^{1:N}$ which form the basis of the applications in Section 5.

Forecasting For out-of-sample time points, a forecast over an h step horizon $T < t < T + h$ is generated by ancestral sampling: first draw a chain $\tilde{s} \sim \text{Uniform}[1 \dots S]$, then simulate step 5 of Figure 2a using the latent variables in chain $\xi^{\tilde{s}}$ for $t = T, \dots, T+h$.

Clustering For a pair of time series $(\mathbf{x}^i, \mathbf{x}^k)$, the posterior probability that they are dependent is the fraction of samples in which they are in the same cluster:

$$\mathbb{P} \left[c^i = c^k \mid \mathbf{x}^{1:N} \right] \approx \frac{1}{S} \sum_{s=1}^S \mathbb{I} [\hat{c}^{i,s} = \hat{c}^{k,s}]. \quad (7)$$

Imputation Posterior inference yields samples of each temporal regime $\hat{z}_t^{i,s}$ for all in-sample time points $1 \leq t \leq T$; the posterior distribution of a missing value is:

$$\mathbb{P} \left[x_t^n \in B \mid \mathbf{x}^{1:N} \setminus \{x_t^n\} \right] \approx \frac{1}{S} \sum_{s=1}^S F(B \mid \hat{\theta}_{\hat{z}_t^{n,s}}^{n,s}). \quad (8)$$

5 Applications

In this section, we apply the TRCRP mixture to clustering hundreds of time series using macroeconomic data from the Gapminder Foundation, as well as imputation and forecasting tasks on seasonal flu data from the US Center for Disease Control and Prevention (CDC). We describe the setup in the text below, with further commentary given in Figures 4, 5, and 6. Experimental methods are detailed in Appendix C¹.

We first applied the TRCRP mixture with hierarchical prior to cluster countries in the Gapminder dataset, which contains dozens of macroeconomic time series for 170 countries spanning 50 years. Because fluctuations due to events such as natural disasters, financial crises, or healthcare epidemics are poorly described by parametric or hand-designed causal models, a key objective is to automatically discover the number and kinds of patterns underlying the tempo-

¹An implementation of the hierarchical TRCRP mixture is available at <https://github.com/probcomp/trcrpm>.

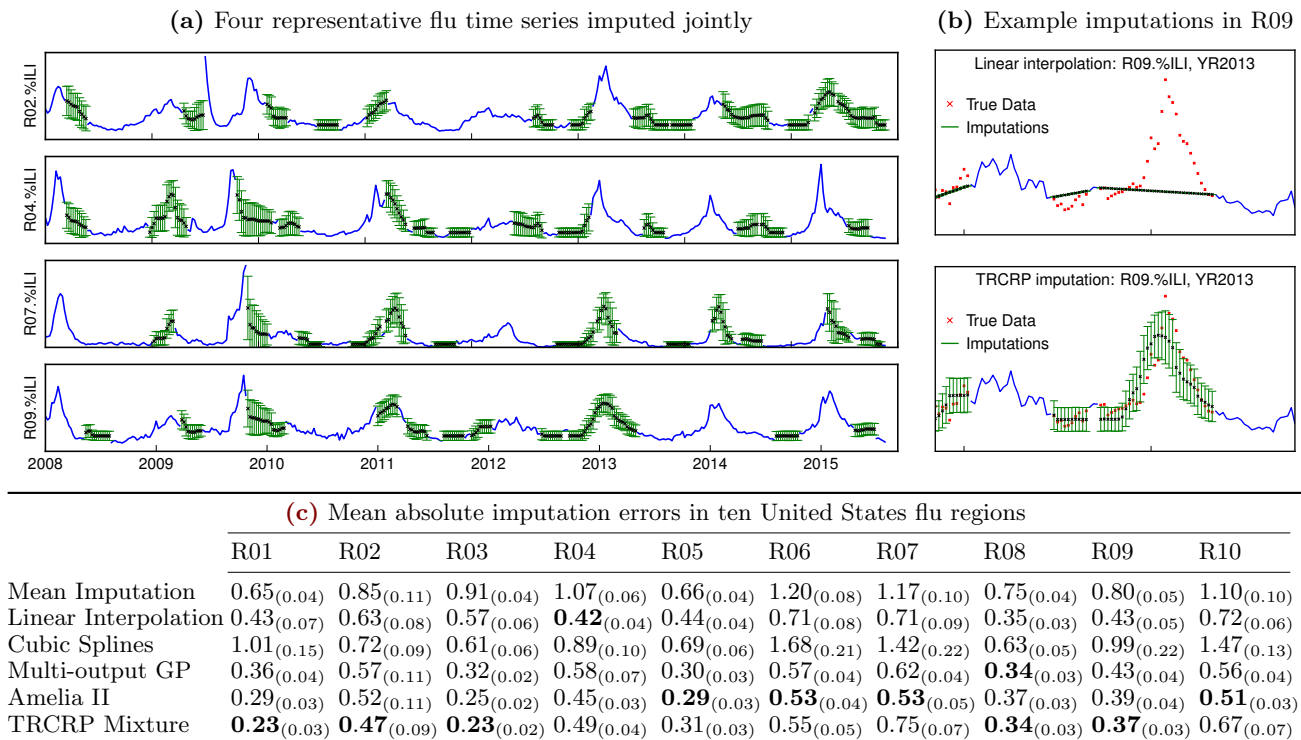


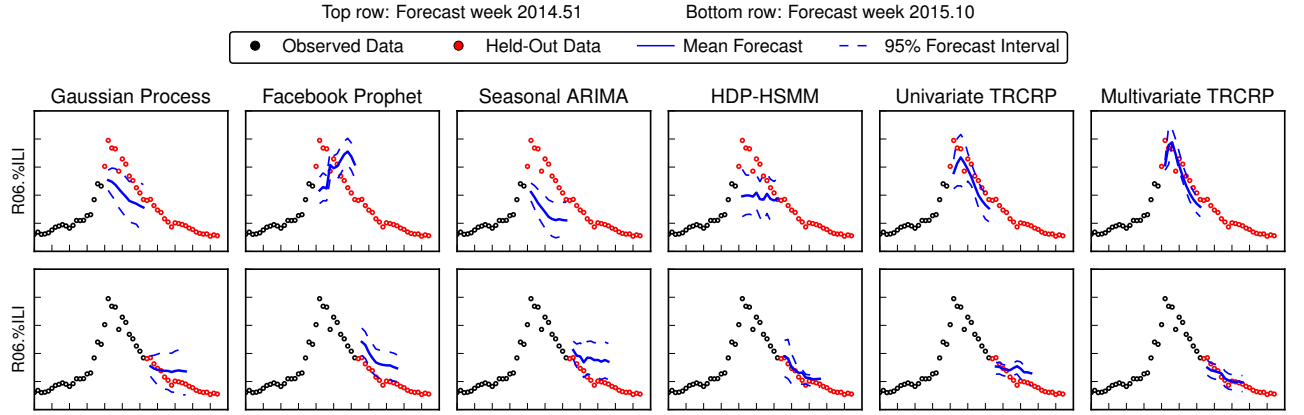
Figure 5: Jointly imputing missing data in ten flu populations over eight seasons. (a) Imputations and standard errors in four of the time series. The TRCRP mixture accurately captures both seasonal behavior as well as non-recurrent characteristics, such as the very mild flu season in 2012. (c) Comparing imputation quality with several baseline methods. The TRCRP mixture ($p = 10$ weeks) achieves comparable performance to Amelia II. Cubic splines are completely ineffective due to long sequences without any observations. (b) While linear interpolation may seem to be a good performer given its simplicity and mean errors, unlike the TRCRP it cannot predict non-linear behavior when an entire flu season is unobserved and entirely misses seasonality.

ral structure. Figure 4 shows the outcome of structure discovery in GDP time series using the model with $p = 5$ years. Several common-sense, qualitatively distinct clusters are detected. Note that countries within each cluster share similar political, economic, and/or geographic characteristics; see caption for additional details. Appendix C.5 gives an expanded set of clusterings showing changepoint detection in cell phone subscription time series, and compares to a baseline using k-medoids clustering.

Predicting flu rates is a fundamental objective in public health policy. The CDC has an extensive dataset of flu rates and associated time series such as weather and vaccinations. Measurements are taken weekly from January 1998 to June 2015. Figure 2b shows the influenza-like-illness rate (ILI, or flu), tweets, and minimum temperature time series in US Region 4, as well as six temporal regimes detected by one posterior sample of the TRCRP mixture model ($p = 10$ weeks). We first investigated the performance of the proposed model on a multivariate imputation task. Windows of length 10 were dropped at a rate of 5% from flu se-

ries in US Regions 1-10. The top panel of Figure 5a shows flu time series for US Regions 2, 4, 7, and 9, as well joint imputations (and two standard deviations) obtained from the TRCRP mixture using (8). Quantitative comparisons of imputation accuracy to baselines are given in Table 5c. In this application, the TRCRP mixture achieves comparable accuracy to the widely used Amelia II [16] baseline, although neither method is uniformly more accurate. A sensitivity analysis showing imputation performance with varying p is given in Appendix C.3.

To quantitatively investigate the forecasting abilities of the model, we next held out the 2015 season for 10 US regions and generated forecasts on a rolling basis. Namely, for each week $t = 2014.40, \dots, 2015.20$ we forecast $\mathbf{x}_{1:t+h}^{\text{flu}}$ given $\mathbf{x}_{1:t-2}^{\text{flu}}$ and all available covariate data up to time t , with horizon $h = 10$. A key challenge is that when forecasting $\mathbf{x}_{t:t+h}^{\text{flu}}$, the most recent flu measurement is two weeks old x_{t-2}^{flu} . Moreover, covariate time series are themselves sparsely observed in the training data (for instance, all Twitter data is missing before June 2013, top panel of Figure 2b).



Mean absolute flu prediction error for 10 forecast horizons (in weeks) averaged over 10 United States flu regions

	$h = 1$	$h = 2$	$h = 3$	$h = 4$	$h = 5$	$h = 6$	$h = 7$	$h = 8$	$h = 9$	$h = 10$
[†] Linear Extrapolation	0.65 _(0.06)	0.79 _(0.05)	0.93 _(0.05)	1.08 _(0.05)	1.24 _(0.05)	1.39 _(0.05)	1.55 _(0.05)	1.70 _(0.05)	1.86 _(0.05)	2.01 _(0.05)
[†] GP(SE+PER+WN)	0.53 _(0.04)	0.60 _(0.03)	0.66 _(0.03)	0.71 _(0.03)	0.75 _(0.02)	0.79 _(0.02)	0.82 _(0.02)	0.85 _(0.02)	0.87 _(0.02)	0.89 _(0.02)
[†] GP(SE×PER+WN)	0.50 _(0.04)	0.57 _(0.03)	0.62 _(0.03)	0.67 _(0.02)	0.71 _(0.02)	0.74 _(0.02)	0.78 _(0.02)	0.81 _(0.02)	0.84 _(0.02)	0.86 _(0.02)
[†] Facebook Prophet	0.83 _(0.04)	0.84 _(0.03)	0.85 _(0.02)	0.85 _(0.02)	0.85 _(0.02)	0.86 _(0.02)	0.86 _(0.02)	0.87 _(0.02)	0.87 _(0.01)	0.87 _(0.01)
[†] Seasonal ARIMA	0.64 _(0.04)	0.76 _(0.03)	0.84 _(0.03)	0.92 _(0.03)	0.98 _(0.03)	1.04 _(0.02)	1.08 _(0.02)	1.13 _(0.02)	1.16 _(0.02)	1.19 _(0.02)
[†] TRCRP Mixture	0.54 _(0.04)	0.58 _(0.03)	0.62 _(0.02)	0.67 _(0.02)	0.71 _(0.02)	0.76 _(0.02)	0.80 _(0.02)	0.83 _(0.02)	0.86 _(0.02)	0.89 _(0.02)
[‡] HDP-HSMM	0.69 _(0.05)	0.72 _(0.04)	0.76 _(0.03)	0.79 _(0.03)	0.82 _(0.02)	0.84 _(0.02)	0.86 _(0.02)	0.88 _(0.02)	0.89 _(0.02)	0.90 _(0.02)
[*] Multi-output GP	0.70 _(0.04)	0.77 _(0.03)	0.84 _(0.03)	0.88 _(0.03)	0.91 _(0.02)	0.93 _(0.02)	0.95 _(0.02)	0.97 _(0.02)	0.99 _(0.02)	1.01 _(0.02)
[*] TRCRP Mixture	0.46 _(0.03)	0.49 _(0.02)	0.51 _(0.02)	0.53 _(0.02)	0.56 _(0.02)	0.58 _(0.02)	0.59 _(0.01)	0.61 _(0.01)	0.62 _(0.01)	0.64 _(0.01)

Modeled time series: [†]flu [‡]flu+weather ^{*}flu+weather+tweets

Figure 6: Quantitative evaluation of forecasting performance on the 2015 flu season. The table shows mean prediction errors and (one standard error) of the flu rate, for various forecast horizons averaged over US Regions 1–10. Available covariate time series include minimum temperature and Twitter messages about the flu (not shown, see Figure 2b). Predictive improvement of the multivariate TRCRP mixture over baselines is especially apparent at longer horizons. The top two panels show sample forecasts in US Region 6 for week 2014.51 (pre-peak) and week 2015.10 (post-peak). The TRCRP mixture accurately forecasts seasonal dynamics in both cases, whereas baseline methods produce inaccurate forecasts and/or miscalibrated uncertainties.

Figure 6 shows the forecasting accuracy from several widely-used, domain-general baselines that do not require detailed custom modeling for obtaining forecasts, and that have varying ability to make use of covariate data (weather and tweet signals). The TRCRP mixture consistently produces the most accurate forecasts for all horizons (last row). Methods such as seasonal ARIMA [17] can handle covariate data in principle, but cannot handle missing covariates in the training set or over the course of the forecast horizon. Both Facebook Prophet [36] and ARIMA incorrectly forecast the peak behavior (Figure 6, top row), and are biased in the post-peak regime (bottom row). The HDP-HSMM [19] also accounts for weather data, but fails to detect flu peaks. The univariate TRCRP (only modeling the flu) performs similarly to periodic Gaussian processes, although the latter gives wider posterior error bars, even in the relatively noiseless post-peak regime. The multi-output GP [3] uses both weather and tweet covariates, but they do not result in an improvement in predictive accuracy over univariate methods.

6 Discussion

This paper has presented the temporally-reweighted CRP mixture, a domain-general nonparametric Bayesian method for multivariate time series. Experiments show strong quantitative and qualitative results on multiple real-world multivariate data analysis tasks, using little to no custom modeling. For certain application domains, however, predictive performance may improve by extending the model to include custom knowledge such as time-varying functionals. Further avenues for research include guidelines for selecting the window size; greater empirical validation; a stick breaking representation; improving inference scalability; and establishing theoretical conditions for posterior consistency. Also, it could be fruitful to integrate this method into a probabilistic programming platform [33], such as BayesDB. This integration would make it easy to query mutual information between time series [32], identify data that is unlikely under the model, and make the method accessible to a broader audience.

Acknowledgments

This research was supported by DARPA PPAML program, contract number FA8750-14-2-0004. The authors wish to thank Max Orhai from Galois, Inc. for assembling the CDC flu dataset.

References

- [1] A. Ahmed and E. Xing. Dynamic non-parametric mixture models and the recurrent Chinese restaurant process: with applications to evolutionary clustering. In *Proceedings of the 2008 SIAM International Conference on Data Mining*, pages 219–230. SIAM, 2008.
- [2] D. J. Aldous. Exchangeability and related topics. In P. L. Hennequin, editor, *École d’Été de Probabilités de Saint-Flour XIII*, pages 1–198. Springer, 1985.
- [3] M. Alvarez and N. D. Lawrence. Sparse convolved Gaussian processes for multi-output regression. In *Advances in Neural Information Processing Systems 21*, pages 57–64. Curran Associates, Inc., 2009.
- [4] D. Barber. Expectation correction for smoothed inference in switching linear dynamical systems. *Journal of Machine Learning Research*, 7(Nov):2515–2540, 2006.
- [5] J. Bernardo and A. Smith. *Bayesian Theory*. Wiley Series in Probability & Statistics. Wiley, 1994. ISBN 9780471924166.
- [6] D. J. Berndt and J. Clifford. Using dynamic time warping to find patterns in time series. In *Workshop on Knowledge Discovery in Databases, AAAIWS-94*, pages 359–370. AAAI Press, 1994.
- [7] D. M. Blei and J. D. Lafferty. Dynamic topic models. In *Proceedings of the 23rd International Conference on Machine learning*, pages 113–120. ACM, 2006.
- [8] F. Caron, M. Davy, A. Doucet, E. Duflos, and P. Vanheeghe. Bayesian inference for linear dynamic models with Dirichlet process mixtures. *IEEE Transactions on Signal Processing*, 56(1):71–84, 2008.
- [9] C. M. Carvalho, M. S. Johannes, H. F. Lopes, and N. G. Polson. Particle learning and smoothing. *Statistical Science*, 25(1):88–106, 02 2010.
- [10] D. B. Dunson, N. Pillai, and J.-H. Park. Bayesian density regression. *Journal of the Royal Statistical Society: Series B (Statistical Methodology)*, 69(2):163–183, 2007.
- [11] M. D. Escobar and M. West. Bayesian density estimation and inference using mixtures. *Journal of the American Statistical Association*, 90(430):577–588, 1995.
- [12] E. Fox, E. B. Sudderth, M. I. Jordan, and A. S. Willsky. Nonparametric Bayesian learning of switching linear dynamical systems. In *Advances in Neural Information Processing Systems 21*, pages 457–464. Curran Associates, Inc., 2009.
- [13] B. D. Fulcher and N. S. Jones. Highly comparative feature-based time-series classification. *IEEE Transactions on Knowledge and Data Engineering*, 26(12):3026–3037, 2014.
- [14] P. J. Green. Reversible jump Markov chain Monte Carlo computation and Bayesian model determination. *Biometrika*, 82(4):711–732, 1995.
- [15] L. F. Gruber and M. West. Bayesian online variable selection and scalable multivariate volatility forecasting in simultaneous graphical dynamic linear models. *Econometrics and Statistics*, 3(C):3–22, 2017.
- [16] J. Honaker, G. King, and M. Blackwell. Amelia II: A program for missing data. *Journal of Statistical Software*, 45(7):1–47, 2011.
- [17] R. Hyndman and Y. Khandakar. Automatic time series forecasting: The forecast package for R. *Journal of Statistical Software*, 27(3):1–22, 2008. ISSN 1548-7660.
- [18] H. Ishwaran and L. F. James. Generalized weighted Chinese restaurant processes for species sampling mixture models. *Statistica Sinica*, 13(4):1211–1235, 2003.
- [19] M. J. Johnson and A. S. Willsky. Bayesian non-parametric hidden semi-Markov models. *Journal of Machine Learning Research*, 14(Feb):673–701, 2013.
- [20] G. M. Koop. Forecasting with medium and large Bayesian VARS. *Journal of Applied Econometrics*, 28(2):177–203, 2013.
- [21] V. Mansinghka, P. Shafto, E. Jonas, C. Petschulat, M. Gasner, and J. B. Tenenbaum. Cross-Cat: A fully Bayesian nonparametric method for analyzing heterogeneous, high dimensional data. *Journal of Machine Learning Research*, 17(138):1–49, 2016.
- [22] P. Mueller and F. Quintana. Random partition models with regression on covariates. *Journal of Statistical Planning and Inference*, 140(10):2801–2808, 2010.
- [23] P. Mueller, F. Quintana, and G. L. Rosner. A product partition model with regression on covariates. *Journal of Computational and Graphical Statistics*, 20(1):260–278, 2011.

- [24] K. P. Murphy. Conjugate Bayesian analysis of the Gaussian distribution. Technical report, University of British Columbia, 2007.
- [25] R. M. Neal. Markov chain sampling methods for Dirichlet process mixture models. *Journal of Computational and Graphical Statistics*, 9(2): 249–265, 2000.
- [26] L. E. Nieto-Barajas and A. Contreras-Cristan. A Bayesian nonparametric approach for time series clustering. *Bayesian Analysis*, 9(1):147–170, 03 2014.
- [27] L. E. Nieto-Barajas and F. A. Quintana. A Bayesian non-parametric dynamic AR model for multiple time series analysis. *Journal of Time Series Analysis*, 37(5):675–689, 2016.
- [28] J.-H. Park and D. B. Dunson. Bayesian generalized product partition model. *Statistica Sinica*, 20(3):1203–1226, 2010.
- [29] C. Ritter and M. Tanner. The griddy Gibbs sampler. Technical Report 878, University of Wisconsin-Madison, 1991.
- [30] H. Robbins. The empirical Bayes approach to statistical decision problems. *The Annals of Mathematical Statistics*, 35(1):1–20, 1964.
- [31] A. Rodriguez and E. ter Horst. Bayesian dynamic density estimation. *Bayesian Analysis*, 3(2):339–365, 6 2008.
- [32] F. Saad and V. Mansinghka. Detecting dependencies in sparse, multivariate databases using probabilistic programming and non-parametric Bayes. In *Proceedings of the 20th International Conference on Artificial Intelligence and Statistics*, volume 54 of *Proceedings of Machine Learning Research*, pages 632–641. PMLR, 2017.
- [33] F. Saad and V. K. Mansinghka. A probabilistic programming approach to probabilistic data analysis. In *Advances in Neural Information Processing Systems 29*, pages 2011–2019. Curran Associates, Inc., 2016.
- [34] U. Schaechtle, B. Zinberg, A. Radul, K. Stathis, and V. Mansinghka. Probabilistic programming with Gaussian process memoization. *arXiv preprint*, arXiv:1512.05665, 2015.
- [35] B. Shahbaba and R. Neal. Nonlinear models using Dirichlet process mixtures. *Journal of Machine Learning Research*, 10(Aug):1829–1850, 2009.
- [36] S. J. Taylor and B. Letham. Forecasting at scale. *The American Statistician*, To appear, 2017.
- [37] Y. W. Teh. Dirichlet process. In *Encyclopedia of Machine Learning*, pages 280–287. Springer, 2011.
- [38] Z. G. Zhu, Xiaojin and J. Lafferty. Time-sensitive Dirichlet process mixture models. Technical Report CMU-CALD-05-104, Carnegie-Mellon University, School of Computer Science, 2005.

Appendices

A Data-dependent parameters for Student-T reweighting function

Following (4), the reweighting function G is a product of p Student-T distributions whose location, scale and degrees of freedom are data-dependent [24]:

$$\begin{aligned}
 & G(\mathbf{x}_{t-p:t-1}; D_{tk}, \lambda_G) \\
 &= \prod_{i=1}^p G_i(x_{t-i}; D_{tki}, \lambda_{Gi}) \\
 &= \prod_{i=1}^p \text{T}_{2a_{tki}} \left(x_{t-i}; m_{tki}, b_{tki} \frac{V_{tki} + 1}{a_{tki}} \right) \quad (9) \\
 & \lambda_{Gi} = (m_{i0}, V_{i0}, a_{i0}, b_{i0}) \\
 & D_{tki} = \{x_{t'-i} : z_{t'} = k, 1 \leq t' < t\} \\
 & n_{tki} = |D_{tki}| \\
 & \bar{x}_{tki} = \frac{1}{n_{tki}} \sum_{t' \in D_{tki}} x_{t'-i} \quad (10) \\
 & V_{tki} = 1/(V_{i0}^{-1} + n_{tki}) \\
 & m_{tki} = V_{tki}(V_{i0}^{-1}m_{i0} + n_{tki}\bar{x}_{tki}) \\
 & a_{tki} = a_{i0} + n_{tki}/2 \\
 & b_{tki} = b_{k0} + \frac{1}{2} (m_{i0}^2 V_{i0}^{-1} + \sum_{t'} x_{t'-i}^2 - m_{itk}^2 V_{tki}^{-1}).
 \end{aligned}$$

B Markov chain Monte Carlo methods for posterior inference

Here, we provide the details of the MCMC method for posterior simulation from the nonparametric mixture model developed in Section 3. As discussed in the main text, conjugacy of F and π_Θ in (3) means we can analytically marginalize parameters $\{\theta_k^n\}$ when defining the generative process of the TRCRP mixture. The model in Figure 2a therefore becomes:

$$\begin{aligned}
 & \alpha \sim \text{Gamma}(1,1) \quad (11) \\
 & \lambda_G^n \sim H_G^n \quad n = 1, 2, \dots, N \\
 & \lambda_F^n \sim H_F^n \quad n = 1, 2, \dots, N \\
 & \mathbf{x}_{-p+1:0}^n := (x_{-p+1}^n, \dots, x_0^n) \quad n = 1, 2, \dots, N \\
 & \Pr [z_t = k \mid \mathbf{z}_{1:t-1}, \mathbf{x}_{t-p:t-1}^{1:N}, \alpha, \lambda_G^{1:N}] \quad t = 1, 2, \dots, T \\
 & \quad \propto \text{CRP}(k \mid \alpha, \mathbf{z}_{1:t-1}) \prod_{n=1}^N G(\mathbf{x}_{t-p:t-1}^n; D_{tk}^n, \lambda_G^n) \\
 & \quad \text{where } D_{tk}^n := \{\mathbf{x}_{t'-p:t'-1}^n \mid z_{t'} = k, 1 \leq t' < t\} \\
 & \quad \text{and } k = 1, \dots, \max(\mathbf{z}_{1:t-1}) + 1 \\
 & x_t^n \mid \{z_t = k, \mathbf{x}_{1:t-1}^{1:N}\} \sim \int_\theta F(\cdot \mid \theta) \pi_\Theta(\theta \mid D_{tk}^n, \lambda_F^n) d\theta \\
 & \quad \text{where } D_{tk}^n := \{\mathbf{x}_{t'}^n \mid z_{t'} = k, 1 \leq t' < t\}. \\
 & \quad n = 1, 2, \dots, N
 \end{aligned}$$

The integration of F against $\pi_\Theta(\theta \mid D_{tk}^n)$ in the right hand-side of the final line evaluates to a Student-T distribution as in (9), whose updates given D_{tk}^n and λ_F^n are identical to those in (10) with $i = 0$.

Inference on temporal regime assignments ($z_t \mid \mathbf{z}_{1:T \setminus t}, \dots$). We first describe how to transition $\mathbf{z}_{1:T}$, assuming the collapsed version of the TRCRP (11) with N time series. Note that since the hierarchical prior (5) for structure learning results in $M = \max(\mathbf{c}^{1:N})$ independent TRCRP mixtures (conditioned on the assignment vector), it suffices to describe inference on $\mathbf{z}_{1:T}$ in one of the mixtures (which keeps notation significantly simpler). Given observations $\mathbf{x}_{-p+1:T}^{1:N}$, the joint likelihood of model (11) is:

$$\begin{aligned}
 & P(\alpha, \lambda_G^{1:N}, \lambda_F^{1:N}, \mathbf{z}_{1:T}, \mathbf{x}_{1:T}^{1:N}; \mathbf{x}_{-p+1:0}^{1:N}, p) \\
 &= \Gamma(\alpha; 1, 1) \left(\prod_{n=1}^N H_G^n(\lambda_G^n) \right) \left(\prod_{n=1}^N H_F^n(\lambda_F^n) \right) \\
 & \quad \prod_{t=1}^T \left[b_t \text{CRP}(z_t \mid \mathbf{z}_{1:t-1}, \alpha) \right. \\
 & \quad \left. \prod_{n=1}^N G(\mathbf{x}_{t-p:t-1}^n; D_{tz_t}^n, \lambda_G^n) F(x_t^n \mid D_{tz_t}^n, \lambda_F^n) \right] \quad (12)
 \end{aligned}$$

The normalizer at time t is given by:

$$\begin{aligned}
 & b_t(\mathbf{x}_{1:t-1}^{1:N}, \mathbf{z}_{1:t-1}) \quad (13) \\
 &= \left(\sum_{k=1}^{K_t} \text{CRP}(k \mid \alpha, \mathbf{z}_{1:t-1}) \prod_{n=1}^N G(\mathbf{x}_{t-p:t-1}^n; D_{tk}^n, \lambda_G^n) \right)^{-1},
 \end{aligned}$$

where $K_t = \max(\mathbf{z}_{1:t-1}) + 1$. Note that the normalizer $b_t(\mathbf{x}_{1:t-1}^{1:N}, \mathbf{z}_{1:t-1})$ ensures the reweighted cluster probabilities sum to one. It will also be convenient to define the predictive density q_t at time t of data $\mathbf{x}_t^{1:N}$, which sums out all possible values of z_t :

$$\begin{aligned}
 & q_t(\mathbf{x}_{1:t}^{1:N}, \mathbf{z}_{1:t-1}) \quad (14) \\
 &= b_t(\mathbf{x}_{1:t-1}^{1:N}, \mathbf{z}_{1:t-1}) \left(\sum_{k=1}^{K_t} \text{CRP}(k \mid \alpha, \mathbf{z}_{1:t-1}) \right. \\
 & \quad \left. \prod_{n=1}^N G(\mathbf{x}_{t-p:t-1}^n; D_{tk}^n, \lambda_G^n) F(x_t^n \mid D_{tk}^n, \lambda_F^n) \right).
 \end{aligned}$$

Let the current state of the Markov chain be $(\alpha, \lambda_G^{1:N}, \lambda_F^{1:N}, \mathbf{z}_{1:T})$. We present two algorithms for sampling the latent regimes assignments. Algorithm 1 is a single-site Metropolis-Hastings procedure that targets $(z_t \mid \mathbf{z}_{1:T \setminus t}, \dots)$ at each step, where we assume that all data in $\mathbf{x}_{1:T}^{1:N}$ are fully observed. Algorithm 2 is an SMC scheme to block sample $(\mathbf{z}_{1:T} \mid \dots)$ using particle learning [9]. Arbitrary observations may be missing, as they are imputed over the course of inference.

Algorithm 1: single-site Metropolis-Hastings. This algorithm proposes $(z_t | \mathbf{z}_{1:T \setminus t}, \dots)$ at each step, assuming fully observed data $\mathbf{x}_{1:T}^{1:N}$. Repeat for $t = 1, 2, \dots, T$:

1. Propose z'_t from the multinomial distribution:

$$\Pr[z'_t = k | \mathbf{z}_{1:T \setminus t}, \mathbf{x}^{1:N}, \alpha] \propto \text{CRP}(k | \alpha, \mathbf{z}_{1:T \setminus t}) \prod_{n=1}^N G(\mathbf{x}_{t-p:t-1}^n; D_{Tk}^n \setminus \{x_t^n\}, \lambda_G^n) F(x_t^n | D_{Tk}^n \setminus \{x_t^n\}, \lambda_F^n), \quad (15)$$

for $k \in \text{unique}(\mathbf{z}_{1:T \setminus t}) \cup \{\max(\mathbf{z}_{1:T \setminus t}) + 1\}$.

2. Compute the MH acceptance ratio $r(z_t \rightarrow z'_t)$, using b_t defined in (13):

$$r(z_t \rightarrow z'_t) = \frac{\prod_{t' > t} b_{t'}(\mathbf{z}_{1:t'-1 \setminus t} \cup z'_t, \mathbf{x}_{1:t'-1}^{1:N})}{\prod_{t' > t} b_{t'}(\mathbf{z}_{1:t'}, \mathbf{x}_{1:t'-1}^{1:N})}. \quad (16)$$

3. Set $z_t \leftarrow z'_t$ with probability $\min(1, r)$, otherwise leave z_t unchanged.

Algorithm 2: block sampling with particle-learning. This algorithm block samples $\mathbf{z}_{1:T}$ without any assumptions on missingness of observations. Let o_t^n be the ‘‘observation indicator’’ so that $o_t^n = 1$ if x_t^n is observed, and 0 if it missing ($n = 1, 2, \dots, N$ and $t = 1, 2, \dots, T$). Let $J > 0$ be the number of particles. Since we will be simulating missing values over the course of inference, we superscript all data with j to indicate the inclusion of any imputed values by particle j .

1. Set $w^j \leftarrow 1$ for $j = 1, 2, \dots, J$

2. Repeat for $t = 1, 2, \dots, T$

- 2.1. Repeat for $j = 1, 2, \dots, J$

- 2.1.1. Sample z_t^j from the multinomial distribution:

$$\Pr[z_t^j = k | \mathbf{z}_{1:t-1}^j, \mathbf{x}^{1:N,j}, \alpha] \propto \text{CRP}(k | \alpha, \mathbf{z}_{1:t-1}^j) \prod_{n=1}^N G(\mathbf{x}_{t-p:t-1}^{n,j}; D_{tk}^{n,j}, \lambda_G^n) \prod_{n=1}^N \left(F(x_t^n | D_{tk}^{n,j}, \lambda_F^n) \right)^{o_t^n}, \quad (17)$$

for $k = 1, 2, \dots, \max(\mathbf{z}_{1:t-1}^j) + 1$.

- 2.1.2. Update particle weight using predictive density q_t defined in (14):

$$w^j \leftarrow w^j q_t \left(\mathbf{x}_{1:t-1}^{1:N,j} \cup \{x_t^n | o_t^n = 1\}, \mathbf{z}_{1:t-1}^j \right). \quad (18)$$

- 2.1.3. For each n such that $o_t^n = 0$, simulate a value $x_t^{n,j} \sim F(\cdot | D_{tz_t^j}^n, \lambda_F^n)$.

- 2.2. If resampling criterion met, then:

- 2.2.1. Resample $(\mathbf{z}_{1:t}^j, \mathbf{x}_{1:t}^{1:N,j})$ proportionally to w^j , $j = 1, 2, \dots, J$.

- 2.2.2. Renormalize weights $w^j \leftarrow w^j / \sum_{j'} w^{j'}$, $j = 1, 2, \dots, J$.

3. Resample $j \sim \text{Categorical}(w^1, \dots, w^J)$ and return $(\mathbf{z}_{1:T}^j, \mathbf{x}_{1:T}^{1:N,j})$.

It is worth discussing the computational trade-offs between MH Algorithm 1 and SMC Algorithm 2. In step 1 of Algorithm 1, (15) is recomputed $K = O(\max(\mathbf{z}_{1:T}))$ times. Each assessment requires $O(Np)$ computations, where the factor of N is the product over the time series, and the factor of p is the cost of assessing G per (4). In step 2, computing the terms $b_{t'}$ in the acceptance ratio (16) requires revisiting $O(T)$ data points. Therefore a single iteration requires $O(TKNp)$ computations, so that the cost of a full sweep over all T time points is $O(T^2KNp)$. Note that it is not necessary to sum over K_t in (13) when computing the $b_{t'}$ terms in (16), since the data in at most two clusters will change when proposing z_t to $z_{t'}$. The sufficient statistics can be updated in constant time using a simple dynamic programming approach.

In practice, we consider several computational approximations that simplify the scaling properties of the single-site MH Algorithm 1. For missing data, rather than evaluate the full model likelihood (12) on imputed data for each $t = 1, \dots, T$, we instead adopt a “data-dependent” prior, similar to the strategy described by [10] in the context of Bayesian density regression. Namely, letting o_t^n be the indicator for having observed x_t^n , we let the reweighting function G consider only those data points that have actually been observed. Therefore, (4) becomes:

$$G(\mathbf{x}_{t-p:t-1}; D_{tk}, \lambda_G) = \prod_{i=1}^p (G_i(x_{t-i}; D_{tki}, \lambda_{Gi}))^{o_t^n - i}. \quad (19)$$

Second, note that the MH proposal (15) is very similar to the Gibbs proposal from Algorithm 3 of [25], except we must account for the temporal coupling so that the transition is guaranteed to leave (12) invariant. Empirical evidence suggest that, when using the proposal (15), acceptance ratios center around one. This observation suggests a good initialization strategy for the Markov chain (prior to running the full MH algorithm): run several rounds of step 1 always accepting the proposal $z_t \rightarrow z'_t$ without computing (16), which eliminates the additional $O(T)$ factor.

Unlike the MH Algorithm 1, the SMC algorithm (2) with requires $O(KNp)$ to assess (17) in step 2.1.1; the total cost of a complete pass through all T data points (step 2) and all J particles (step 2.1) is therefore $O(JTKNp)$. Note that in SMC, the normalizers b_t need not to be retroactively computed, which is the key overhead of MH. In addition to its linear scaling in T , SMC is able to (i) more tractably handle missing data, and (ii) use a posterior particle filter by sampling from the conditionally optimal proposal distribution in step 2.1.1, resulting in significantly lower variance of the weights [9].

Inference on time series cluster assignments ($c^n | \mathbf{c}^{1:N \setminus n}, \dots$). This section describes an MCMC algorithm for sampling the time series cluster assignments when using the hierarchical CRP structure prior (5). For notational simplicity, let $B \subseteq [N]$ and define:

$$L^m(\mathbf{z}_{1:T}, \mathbf{x}_{1:T}^B) = \prod_{t=1}^T \left[b_t \text{CRP}(z_t | \mathbf{z}_{1:t-1}, \alpha^m) \prod_{n=1}^N G(\mathbf{x}_{t-p:t-1}^n; D_{tz_t}^n, \lambda^n) F(x_t^n | D_{tz_t}^n, \lambda_F^n) \right]. \quad (20)$$

The term L^m is a short-hand for the product from $t = 1$ to T in the full model likelihood (12) for a single TRCRP mixture, with latent sequence $\mathbf{z}_{1:T}$, data $\mathbf{x}_{1:T}^B$, and CRP concentration α^m . Second, let $A^m = \{n | c^n = m\}$ be the indices of the time series currently assigned to cluster m .

Algorithm 3: Sampling time series cluster assignments. Let the current state of the Markov chain be $(\alpha_0, \mathbf{c}^{1:N}, \alpha^{1:M}, \lambda_G^{1:N}, \lambda_F^{1:N}, \mathbf{z}_{1:T}^{1:M})$ with observations $\mathbf{x}_{1:T}^{1:N}$. This algorithm resamples $(c^n | \mathbf{c}^{1:N \setminus n}, \dots)$. Repeat for $n = 1, 2, \dots, N$:

1. If c^n is not a singleton cluster, i.e. $|A^{c^n}| > 1$, then generate a proposal sequence by forward sampling $\mathbf{z}_{1:T}^{M+1}$ from model prior (11), holding the data $\mathbf{x}_{1:T}^n$ fixed at the observed values.

2. If c^n is a singleton, i.e. $|A^{c^n}| = 1$, then re-use the current latent regime sequence by setting $\mathbf{z}_{1:T}^{M+1} = \mathbf{z}_{1:T}^{c^n}$

3. For $m \in \text{unique}(\mathbf{c}^{1:N \setminus n})$, compute

$$p^m = \begin{cases} |A^m| L^m(\mathbf{z}_{1:T}^m, \mathbf{x}_{1:T}^n) & \text{if } c^n \neq m, \\ (|A^m| - 1) L^m(\mathbf{z}_{1:T}^m, \mathbf{x}_{1:T}^n) & \text{if } c^n = m. \end{cases}$$

4. Compute the singleton proposal probability:

$$p^{M+1} = \alpha_0 L_{M+1}(\mathbf{z}_{1:T}^{M+1}, \mathbf{x}_{1:T}^n)$$

5. Sample $c' \sim \text{Categorical}(\{p^m\})$.

6. Compute the MH acceptance ratio

$$r(c^n \rightarrow c') = \left(\frac{L^{c'}(\mathbf{z}_{1:T}^{c'}, \mathbf{x}_{1:T}^{A^{c'}} \cup \mathbf{x}_{1:T}^n) L^{c^n}(\mathbf{z}_{1:T}^{c^n}, \mathbf{x}_{1:T}^{A^{c^n}} \setminus \mathbf{x}_{1:T}^n)}{L^{c'}(\mathbf{z}_{1:T}^{c'}, \mathbf{x}_{1:T}^{A^{c'}}) L^{c^n}(\mathbf{z}_{1:T}^{c^n}, \mathbf{x}_{1:T}^{A^{c^n}})} \right) \left(\frac{L^{c^n}(\mathbf{z}_{1:T}^{c^n}, \mathbf{x}_{1:T}^n)}{L^{c'}(\mathbf{z}_{1:T}^{c'}, \mathbf{x}_{1:T}^n)} \right). \quad (21)$$

7. Set $c^n \leftarrow c'$ with probability $\min(1, r)$, else leave c^n unchanged.

By proposing the latent regime singleton from the (conditional) prior in Step 2 of Algorithm 3, transdimensional adjustments such as reversible jump MCMC [14] need not be considered. Second, when computing the MH acceptance ratio (21) in step 6, it is not necessary to recompute all the L^m terms at each iteration. First, writing out the full products (20) results in cancellation of several terms in the numerator and denominator of (21). Second the b_t^m terms that do not cancel contain several duplicated components, which can be reused from one transition to the other.

In practice, we find that a similar heuristic to the one described for Algorithm 1 provides good transitions in the state space, given the similarities between Algorithm 3 and the Gibbs Algorithm 8 from [25].

Inference on model hyperparameters ($\alpha_0, \{\alpha^m\}, \{\lambda_G^n\}, \{\lambda_F^n\} | \dots$). This section describes the empirical Bayes approach [30] for transitioning model hyperparameters, using the “griddy Gibbs” approach from [29]. For each hyperparameter, we construct a grid of 30 data-dependent logarithmically-spaced bins as follows:

Outer CRP concentration

$$\text{grid}(\alpha_0) = \text{logspace}(1/N, N)$$

TRCRP concentration

$$\text{grid}(\alpha^m) = \text{logspace}(1/T, T)$$

Normal-InverseGamma hyperparameters

$$\begin{aligned} \text{grid}(m_0^n) &= \text{logspace}(\min(\mathbf{x}_{1:T}^n) - 5, \max(\mathbf{x}_{1:T}^n) + 5) \\ \text{grid}(V_0^n) &= \text{logspace}(1/T, T) \\ \text{grid}(a_0^n) &= \text{logspace}(\text{ssqdev}(\mathbf{x}_{1:T}^n)/100, \text{ssqdev}(\mathbf{x}_{1:T}^n)) \\ \text{grid}(b_0^n) &= \text{logspace}(1, T). \end{aligned}$$

Grids for the Normal-InverseGamma hyperparameters apply to both λ_F ($n = 1, 2, \dots, N$) and λ_G (windows $i = 1, 2, \dots, p$). We cycle through the grid points of each hyperparameter, and assess the conditional likelihood at each bin using (6). We find that this method is both computationally reasonable and finds good hyperparameter settings. However, alternative approaches based on slice sampling offer a promising alternative to achieve fully Bayesian inference over hyperparameters.

C Experimental Methods

This section describes the quantitative experimental methods used for forecasting, clustering, and imputation pipelines in Section 5. Access to experimental pipeline code is available upon request.

C.1 Flu forecasting

The full CDC flu datasets used in this paper are available at <https://github.com/GaloisInc/ppaml-cp7/tree/master/data>. Flu populations were constructed from the following csv files: USA-flu.csv, USA-tweets.csv, and USA-weather.csv. In each of US Regions 1 through 10, we held out data from weeks 2014.40 through 2015.20, and produced forecasts with a 10 week horizon on a rolling basis. Tweet and minimum temperature covariates were used. More precisely, for a region r (such as US Region 10) a forecaster F for week t extending h weeks into the future is a function:

$$F_{r,t,h} : \left\{ \mathbf{x}_{1:t-2}^{\text{flu},r}, \mathbf{x}_{1:t}^{\text{cov},r} \right\} \mapsto \left\{ \mathbf{x}_{t:t+h}^{\text{flu},r} \right\}. \quad (22)$$

The forecasters iterated over regions $r = 1, 2, \dots, 10$, weeks $t = 2014.40, 2014.41, \dots, 2015.20$, and horizons $h = 1, 2, \dots, 10$. Note that the two week delay in the latest flu data is expressed by only having data up to $t-2$ when forecasting at week t . Second, \mathbf{x}^{cov} contains arbitrary missing values (see for example the tweets time series from Figure 2b). When forecasting, covariate values are only available up to the current week t , not the entire course of the forecast horizon. Nine forecasting methods were used in the paper, shown in Figure 6. Below are further details on each forecaster:

Constant. This method returns a constant prediction based on the most recently observed flu value x_{t-2}^{flu} over the entire course of the horizon.

Linear extrapolation. This method fits a straight line through the three most recently observed flu values, $\mathbf{x}_{t-4:t-2}^{\text{flu}}$, and returns predictions by extrapolating the line for h weeks.

GP (SE+PER+WN). This method is a Gaussian process whose covariance kernel is a sum of squared exponential, periodic, and white noise components. Hyperparameter inference was conducted using the open source implementation from the Venture platform [34; <https://github.com/probcomp/Venturecxx>]. MH sampling on data-dependent hyperparameter grids were run for a burn-in period of 10000 iterations. Predictions were obtained by drawing 500 independent curves from the posterior predictive distribution, evaluated jointly at the forecast weeks.

GP (SE×PER+WN). Identical to above, except to using a covariance kernel with a product of squared exponential and periodic components, plus white noise. The change in covariance kernel resulted in little quantitative and qualitative differences.

Facebook Prophet. We used the open-source python implementation of Facebook Prophet [36; <https://facebook.github.io/prophet>]. We specified the data sampling rate as weekly. The method requires

no additional specification or tuning. The predictor returns point estimates, as well as upper and lower confidence intervals, at the held-out weeks.

Seasonal ARIMA. We used the R implementation of seasonal ARIMA from the `forecast` package [17; <https://cran.r-project.org/web/packages/forecast>]. The model is parameterized as $\text{ARIMA}(p, d, q)(P, D, Q)_m$, where p is the non-seasonal AR order, d is the non-seasonal differencing, q is the non-seasonal MA order, P is the seasonal AR order, D is the seasonal differencing, Q is the seasonal MA order, and m is the sampling frequency per period. For each of the 10 flu seasons, we used `auto.arima` to perform model selection. We manually specified the weekly sampling rate by setting $m = 52$, and set $D = 1$ to specify 1 flu season per year. The program optimize all other parameters using non-stepwise grid search, which is significantly slower to fit than stepwise search, but is both more extensive and more appropriate for data with seasonal behavior (according to the package documentation). While `auto.arima` can in principle support covariate data using the `xreg` parameter, we were unable to successfully use `xreg` due to missing data in the matrix of external regressors (tweets and weather) at the held-out weeks. The predictor returns point estimates, as well as upper and lower confidence intervals, at the held-out weeks.

Multi-output GP This method is a single-input (time) multiple-output (flu, tweets, and weather data) Gaussian process. We used the the open source MATLAB implementation of sparse convolved Gaussian process for multi-output regression from the `multigp` package [3; <https://github.com/SheffieldML/multigp>]. We used the following configuration options:

```
i multigpOptions('ftc');
ii options.kernType='ggwhite';
iii options.optimizer='scg';
iv options.nlf=1,
```

to specify (i) full estimation without running likelihood approximations; (ii) a Gaussian-Gaussian kernel with white noise; (iii) scaled conjugate gradient optimization; and (iv) one latent function. Moreover, the `options.bias` and `options.scale` parameters were initialized to their empirical values from the training set. Optimization was run until convergence for all forecasters. This method is the only baseline which can handle arbitrary patterns of missing data, thereby making use of the weather and tweet signals when forecasting predictions at time t . However, the absence of a periodic kernel in the convolved GP implementation made it difficult to capture the seasonal dynamics. Predictions were obtained by sampling 500 inde-

pendent normal random variables from the posterior predictive distribution evaluated at the forecast weeks.

HDP-HSMM. This method is the hierarchical Dirichlet process semi-Markov model; experiments were run using the open-source python package `pyhsmm` [19; <https://github.com/mattjj/pyhsmm>]. While the HDP-HSMM cannot handle missing values in the training data, it can handle missing data over the course of the prediction horizon. Therefore, flu and weather time series were modeled jointly, leaving out the tweets. We used the `WeakLimitHDPHSMM` model, with a Poisson duration distribution and Gaussian observation distribution. Default configurations of all hyperparameters of these distributions and the HDP-HSMM concentration were taken from examples made available by the authors. MCMC inference with 1000 steps of burn-in was used. Predictions were obtained by drawing 100 independent curves from the posterior predictive evaluated at the forecast weeks.

Univariate TRCRP mixture. This method only considered the flu time series using model (2). We used a window size of $p = 10$ weeks, and $S = 64$ parallel MCMC runs with a burn-in period of 5000 iterations. Predictions were obtained by drawing 500 independent curves from the posterior predictive distribution evaluated at the forecast weeks.

Multivariate TRCRP mixture. This method considered flu, weather and tweet time series using the model in Figure 2a. We used a window size of $p = 10$ weeks, and $S = 64$ parallel MCMC runs with a burn-in period of 5000 iterations. Missing covariate data was handled using the approximation given in (19). Using the hierarchical structure prior (5) resulted in little to no quantitative difference. The three time series are dependent, which was reflected in their posterior dependence probability (7) being 1 across all 64 independent chains. Predictions were obtained by sampling 500 independent curves from the posterior predictive distribution evaluated at the forecast weeks. An open-source implementation of the method used in this paper is at <https://github.com:probcomp/trcrpm>.

C.2 Flu imputation

We constructed a single population of 10 flu time series for US Regions 1 through 10. Missing data was dropped independently in each time series by removing consecutive windows of length 10 at a rate of 5%. The full and dropped datasets used for benchmarking are shown in Figure 8. Below are further on details on each of the five imputation methods:

Mean imputation. This method returns the per-series mean as the imputed value for each data point.

Linear interpolation. This method constructs a straight line between every pair of time points $t_1 < t_2$ which have at least one missing observation between them. The interpolation method used was `pandas.Series.interpolate` from the python `pandas` package at <https://pandas.pydata.org>.

Cubic interpolation. The cubic interpolation routine used was `scipy.interpolate.interp1d` from the python `scipy` package at <https://scipy.org>.

Amelia II. This method uses the R package `amelia` [16; <http://cran.r-project.org/web/packages/Amelia>] for multiple imputation. We used 100 samples per missing data point. Imputation errors were averaged over the multiple imputations.

Multivariate TRCRP mixture. A window of $p = 10$ weeks was used, with $S = 64$ parallel MCMC runs and a burn-in period of 5000 iterations. 100 predictive samples from each of the chains were obtained using (8), and imputation errors were averaged over the multiple imputations. Joint imputations of Regions 1 through 10 are shown Figure 8.

C.3 Sensitivity of imputation performance to the TRCRP mixture window size

We further studied how imputation performance of the TRCRP mixture varied as we changed the window size p . Figure 7 shows the outcome of this sensitivity analysis. In all cases, the sampler was run for a burn-in of 5000 iterations with $S = 16$ chains. While imputation is generally not highly sensitive to p , median imputation values degrades slightly with increasing p and the variance of imputation errors increases. (At higher p , the MCMC chains need a significantly higher number of iterations to mix well than at lower p .)

The reason that small p works well for jointly imputing the 10 time series in Figure 8 is that the multivariate TRCRP mixture shares statistical strength across time series. Namely, when imputing a missing value $x_t^{n_0}$ at time t for time series n_0 , the relevant variables for predicting the hidden state z_t are (i) the history $\mathbf{x}_{t-p:t-1}^{n_0}$ of the current time series; and (ii) values $\{x_t^n \mid n_0 \neq n\}$ of other time series at time t . The latter effect is the dominant one in this imputation problem, leading to less sensitivity to p than might be expected.

C.4 Clustering GDP time series

The clustering results from Figure 4 were obtained by using a TRCRP with a window of $p = 5$ years. The nine clusters that are shown were obtained by averaging dependence probabilities over $S = 60$ posterior samples (using a burn-in of 5000 iterations), and extracting groups of variables whose dependence proba-

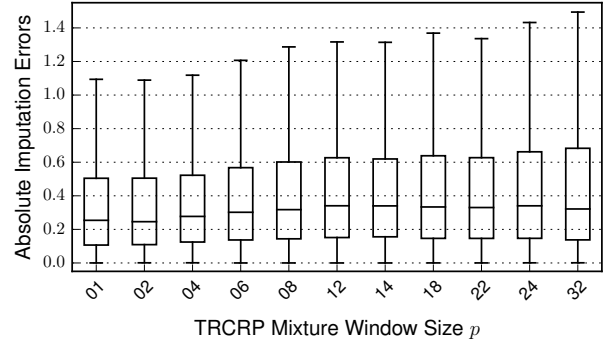


Figure 7: Sensitivity of imputation performance to TRCRP window size p .

bilities (7) exceeded 80%. All time series in Figure 4 are linearly rescaled to $[0, 1]$ for plotting purposes only.

While clustering is an unsupervised task that is challenging to evaluate quantitatively (especially for real-world data, where there is no “ground-truth”), qualitative comparisons to k-medoids clustering with the dynamic time warping metric on the same GDP time series are shown and discussed in Figure 9.

C.5 Expanded results on clustering cell phone subscription time series

In addition to clustering GDP series from Figure 4, we applied the TRCRP prior with hierarchical extension (5) to cluster historical cell phone subscription data. The outcome of the clustering is shown in Figure 10, where we show all 170 time series in the left most figure, along with three representative clusters from one posterior sample. Each cluster corresponds to countries whose change point in cell phone subscribers from zero to non-zero fell in a distinct window: 1985-1995 in cluster 1, 1995-2000 in cluster 2, and 2000-2005 in cluster 3. We also compare renderings of the pairwise dependence probability matrix with the pairwise cross-correlation matrix. Refer to the caption of Figure 10 for additional details.

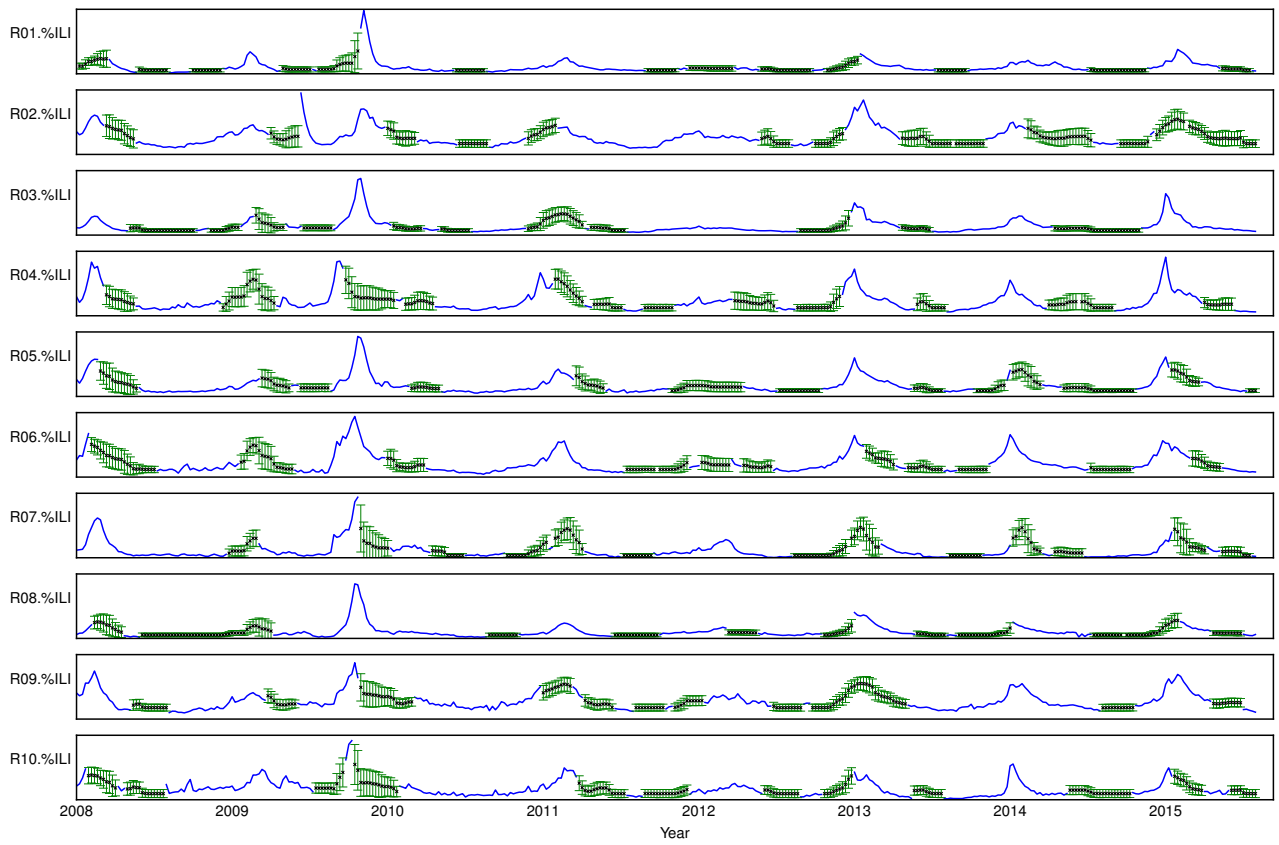
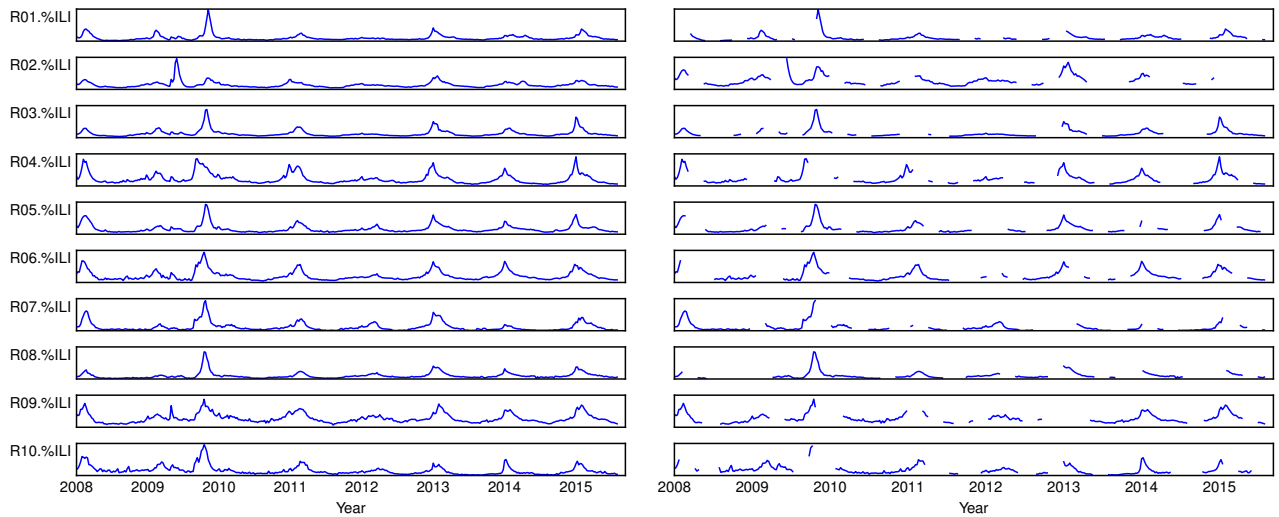


Figure 8: Full, missing, and imputed flu time series over eight years in US Regions 1 through 10.

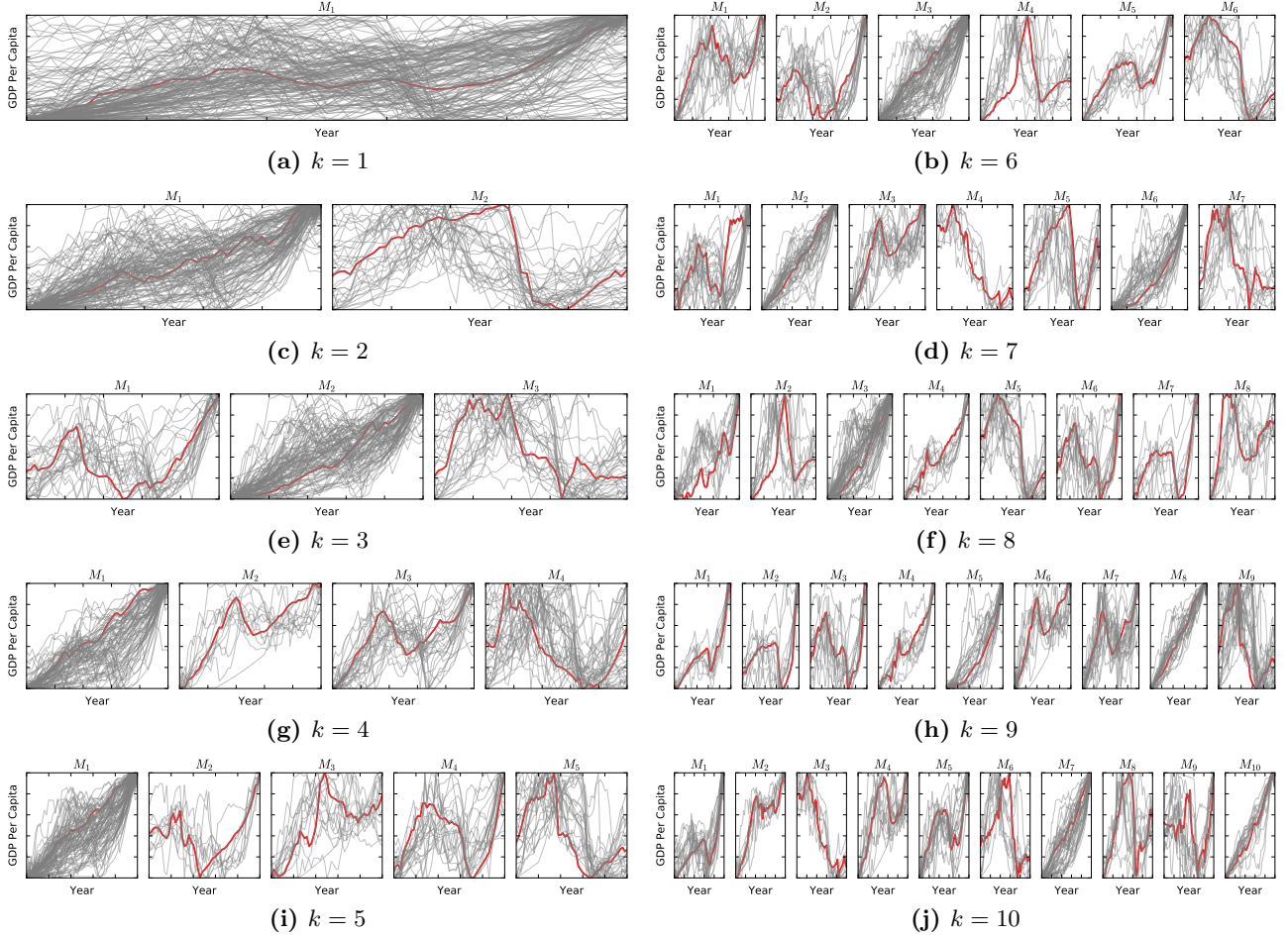
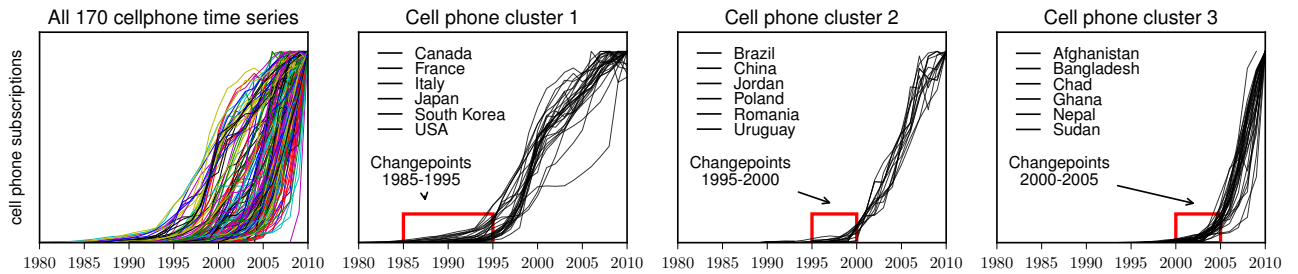
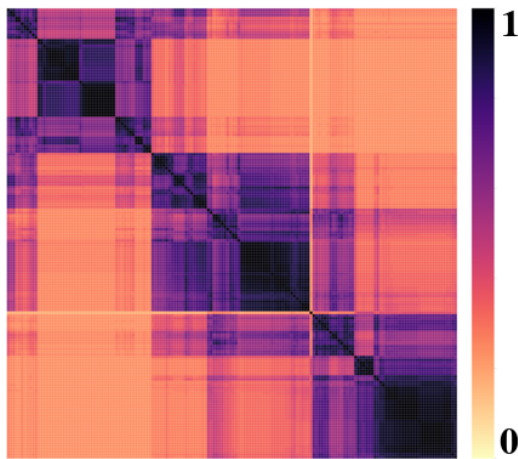


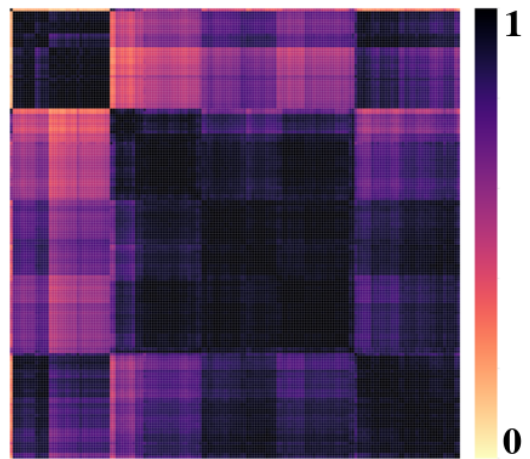
Figure 9: Outputs of k -medoids clustering on the GDP per capita time series for all 170 countries in the Gapminder dataset, with $k = 1, 2, \dots, 10$. Distances are computed using the dynamic time warping (DTW) metric, a common similarity measure between a pair of time series [6]. For each k , we randomly initialized the medoids and ran the algorithm to convergence (medoids are shown in red, and time series assigned to that medoid in gray). Using k -medoids requires hand-tuning the number of latent clusters k , whereas the proposed method (whose posterior clustering is shown in Figure 4 of the main text), places a non-parametric Bayesian prior over this parameter. Moreover, when compared to the clusters detected by the proposed method, those detected by k -medoids with DTW appear qualitatively less distinct, and have more repetitive and duplicated temporal patterns (especially apparent at higher k). Finally, k -medoids outputs a fixed cluster assignment for each time series in the population; these assignments are sensitive to the random initialization and cannot be aggregated in a principled way. In contrast, inference in the proposed method assigns probabilistic cluster assignments that can be averaged coherently using (7) to express posterior uncertainty.



(a) Three posterior clusters in the TRCRP mixture correspond to three non-overlapping change point windows.



(b) Pairwise dependence probability heatmap



(c) Pairwise cross-correlation heatmap

Figure 10: Discovering changepoint patterns in cell phone subscriptions for 170 countries in the Gapminder dataset. (a) The three clusters (extracted from one posterior sample) correspond to three regimes each with non-overlapping change point windows, annotated by red boxes. The representative countries in each cluster have similar adoption times of cell phone technology, a feature which differs across the clusters. (b) and (c) The matrix of dependence probabilities (averaged over 60 posterior samples using (7)) and the matrix of pairwise cross-correlations (bottom) between all pairs 170 time series. Each row and column is a time series, and the color of a cell (a value between 0,1) indicates the posterior dependence probability, resp. cross-correlation coefficient (significant at the 0.05 level with Bonferroni correction). The TRCRP mixture detects more refined dependence structures than those captured by linear statistics.